Contents lists available at SciVerse ScienceDirect



Journal of Molecular Spectroscopy



journal homepage: www.elsevier.com/locate/jms

Fourier transform emission spectra of the $A^2\Pi\to X^2\Sigma^+$ and $B^2\Sigma^+\to X^2\Sigma^+$ band systems of CaH

Alireza Shayesteh^{a,*}, Ram S. Ram^{b,c}, Peter F. Bernath^{c,d,*}

^a School of Chemistry, College of Science, University of Tehran, Tehran 14176, Iran

^b Department of Chemistry and Biochemistry, University of Arizona, Tucson, AZ 85721, USA

^c Department of Chemistry, University of York, Heslington, York YO10 5DD, UK

^d Department of Chemistry and Biochemistry, Old Dominion University, Norfolk, VA 23529, USA

ARTICLE INFO

Article history: Received 11 February 2013 Available online 29 April 2013

Keywords: CaH Fourier transform spectroscopy Electronic transitions Deperturbation

ABSTRACT

High resolution Fourier transform emission spectra of CaH have been recorded in the 12000–17000 cm⁻¹ spectral region, containing several bands of the $A^2\Pi \rightarrow X^2\Sigma^+$ and $B^2\Sigma^+ \rightarrow X^2\Sigma^+$ transitions. The $\Delta v = 0$ sequence bands of both electronic transitions, and the $\Delta v = -1$ sequence bands of the $A \rightarrow X$ band system were observed and rotationally analyzed. The v = 1, 2 and 3 levels of the $A^2\Pi$ state are perturbed system-atically with the v = 0, 1 and 2 levels of the $B^2\Sigma^+$ state, respectively. Deperturbation of the $A^2\Pi$ and $B^2\Sigma^+$ states was carried out using a Hamiltonian matrix that includes ${}^2\Pi$ and ${}^2\Sigma^+$ matrix elements, as well as off-diagonal elements that couple the vibrational levels of the two states. Empirical band constants and Dunham-type parameters were obtained by least-squares fitting of the data. The equilibrium constants T_e , ω_e and $\omega_e x_e$ of 40 CaH were determined to be 14406.877(1), 1336.323(3) and 20.244(2) cm⁻¹ for the $A^2\Pi$ state, and 15756.265(2), 1296.517(3) and 26.121(1) cm⁻¹ for the $B^2\Sigma^+$ states are 1.98212(1) and 1.95778(2) Å, respectively.

© 2013 Elsevier Inc. All rights reserved.

1. Introduction

Calcium hydride is among the most important diatomic molecules in astrophysics [1,2]. The orange and red bands of CaH, i.e., the $A^2\Pi - X^2\Sigma^+$ and $B^2\Sigma^+ - X^2\Sigma^+$ electronic transitions, are found frequently in various stellar environments including sunspots, cool stars and M and L subdwarfs [3–8].

Spectroscopic studies on the A² Π -X² Σ ⁺ and B² Σ ⁺-X² Σ ⁺ systems of CaH began in the 1920s [9–13], and were extended significantly by Berg, Klynning, Kaving, Lindgren, Martin and others in the 1970s [14–21]. The $\Delta v = 0$ and -1 sequences of the A \leftarrow X system, and the $\Delta v = 0$ and +1 sequences of the B \leftarrow X system were detected and rotationally analyzed [14–17]. Strong perturbations were observed between the A² Π (v = 1) and B² Σ ⁺ (v = 0) states, and due to similar vibrational level spacings in the A and B states, all vibrational levels of the B² Σ ⁺ state (v_B) are perturbed strongly by those of the A² Π state ($v_A = v_B + 1$). Several other electronic transitions of CaH involving the X² Σ ⁺ ground state and the low-lying excited states C² Σ ⁺, D² Σ ⁺, E² Π , K² Σ ⁺ and L² Π were also studied

in detail [18–21]. Spectroscopic data from both CaH and CaD were combined by Martin [22], in order to generate a set of empirical potential energy curves for the low-lying ${}^{2}\Sigma^{+}$ states of CaH. The microwave, millimeter-wave, and infrared spectra of CaH have been recorded, and accurate molecular constants have been obtained for the X² Σ^{+} ground state [23–26]. Recently, Shayesteh et al. combined their high resolution Fourier transform infrared data on CaH with all previous ground state data on CaH and CaD, and performed a multi-isotopologue Dunham fit for the X² Σ^{+} state [27].

Parallel to experimental studies, several ab initio calculations have been carried out on calcium hydride. Potential energy curves for the ground state and low-lying excited states were computed and spectroscopic constants, dissociation energies, and equilibrium internuclear distances were reported [28–34]. Accurate electronic excitation energies and dipole moments have been calculated more recently [35–37], and a pure theoretical line list for the $A^2\Pi - X^2\Sigma^+$ and $B^2\Sigma^+ - X^2\Sigma^+$ transitions along with their oscillator strengths have been produced [38].

High resolution spectroscopy on CaH has continued in recent years by the work of Steimle and coworkers who generated a molecular beam of CaH and measured low-*J* lines of the A² Π -X² Σ ⁺ and B² Σ ⁺-X² Σ ⁺ transitions by laser-induced fluorescence with and without external electric and magnetic fields [39–41].

^{*} Corresponding authors. Address: Department of Chemistry and Biochemistry, Old Dominion University, Norfolk, VA 23529, USA (P.F. Bernath).

E-mail addresses: ashayesteh@ut.ac.ir (A. Shayesteh), pbernath@odu.edu (P.F. Bernath).

^{0022-2852/\$ -} see front matter @ 2013 Elsevier Inc. All rights reserved. http://dx.doi.org/10.1016/j.jms.2013.04.009

Lifetimes of the $\nu = 0$ and $\nu = 1$ of the $A^2\Pi$ state of CaH have been measured using time-resolved laser spectroscopy [42]. Fourier transform emission spectra of the $E^2\Pi \rightarrow X^2\Sigma^+$ transitions of CaH and CaD have been reported and the Einstein *A* coefficients have been calculated by Bernath and coworkers [43,44]. The $A^2\Pi \rightarrow X^2\Sigma^+$ and $B^2\Sigma^+ \rightarrow X^2\Sigma^+$ emission spectra of CaD were recorded using a Fourier transform spectrometer and rotationally analyzed to determine Dunham-type constants for the $A^2\Pi$ and $B^2\Sigma^+$ states of CaD [45]. In this paper, we present high resolution emission spectra of the $A^2\Pi \rightarrow X^2\Sigma^+$ and $B^2\Sigma^+ \rightarrow X^2\Sigma^+$ transitions of CaH, recorded with a Fourier transform spectrometer, and report a rotational analysis and deperturbation of the $A^2\Pi$ and $B^2\Sigma^+$ excited states.

2. Experimental details

The visible spectra of CaH were generated using a calcium hollow-cathode lamp operated with 230 V, 640 mA current. A mixture of about 2 Torr of Ne and 110 mTorr of H₂ flowed through the lamp in order to produce the visible region bands of CaH with sufficient signal-to-noise ratio. The emission from the lamp was observed with the 1-m Fourier transform spectrometer associated with the McMath-Pierce Solar Telescope of the National Solar Observatory. The spectrometer was equipped with a visible beamsplitter and Si superblue diode detectors. The spectra in the 10000–20000 cm⁻¹ wavenumber region were recorded at 0.02 cm⁻¹ resolution by coadding 18 scans in about 2.5 h of integration. The spectra were calibrated using the measurements of Ne atomic lines made by Palmer and Engleman [46]. We expect the absolute accuracy of the wavenumber scale to be better than 0.002 cm^{-1} . Overviews of the observed A \rightarrow X and B \rightarrow X bands of CaH are displayed in Figs. 1 and 2, respectively.

Another visible spectrum of CaH was generated using a discharge–furnace emission source at the University of Waterloo. About 50 grams of calcium was placed inside an alumina tube and heated to about 780 °C. The tube was evacuated by a rotary pump, and a mixture of argon and hydrogen (~1.5 Torr) flowed through the cell. A dc discharge was struck between stainless-steel electrodes located at each end of the tube. CaF₂ lenses and windows were used to focus emission of the source onto the entrance aperture of a Bruker IFS 120 HR Fourier transform spectrometer. The spectral range was limited to 8000–15798 cm⁻¹ using an appropriate long-wave-pass filter and the spectrum was recorded

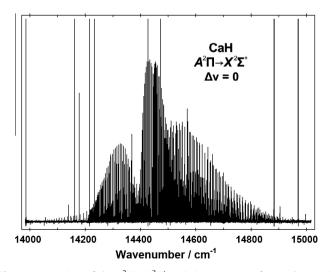


Fig. 1. An overview of the $A^2\Pi\to X^2\Sigma^*$ emission spectrum of CaH: the $\Delta\nu$ = 0 sequence.

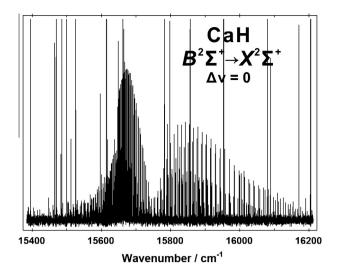


Fig. 2. An overview of the $B^2\Sigma^*\to X^2\Sigma^*$ emission spectrum of CaH: the $\Delta\nu$ = 0 sequence.

using a silicon photodiode detector with an instrumental resolution of 0.05 cm⁻¹. About 200 scans were co-added to improve the signal-to-noise ratio. A small portion of this spectrum showing the $\Delta v = -1$ sequence of the A \rightarrow X transition is displayed in Fig. 3. Line positions were measured using the program WSPECTRA written by Carleer, and air-vacuum correction was done using the formula given by Hirao et al. [47]. About 300 strong unblended lines of CaH were used to calibrate this spectrum against the first one. We performed another independent calibration for this spectrum using argon atomic lines [48,49], and found that the two calibration factors agree very well; they differed by 1×10^{-9} which corresponds to a difference of less than 0.0002 cm⁻¹ in CaH line positions.

3. Results and analysis

We used the first spectrum (higher resolution) for all $B^2\Sigma^+ \rightarrow X^2\Sigma^+$ bands and the $\Delta v = 0$ sequence of the $A^2\Pi \rightarrow X^2\Sigma^+$ bands, while the second spectrum was used only for the $\Delta v = -1$ sequence of the $A^2\Pi \rightarrow X^2\Sigma^+$ system. Overall, the 0–0, 1–1, 2–2,

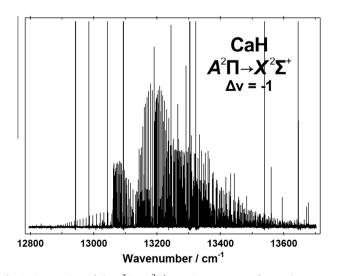


Fig. 3. An overview of the $A^2\Pi \to X^2\Sigma^*$ emission spectrum of CaH: the Δv = -1 sequence.

3-3. 0-1. 1-2. 2-3 and 3-4 bands of the $A^2\Pi \rightarrow X^2\Sigma^+$ transition. and the 0–0, 1–1 and 2–2 bands of the $B^2\Sigma^+ \rightarrow X^2\Sigma^+$ transition of CaH were assigned. Table 1 lists the highest rotational quantum number observed (assigned) for the vibrational levels of the $A^2\Pi$ and $B^2\Sigma^+$ states. Origins of the $\Delta v = 0$ bands of the $A^2\Pi \rightarrow X^2\Sigma^+$ system are $T_{00} = 14425.564$, $T_{11} = 14461.147$, $T_{22} = 14494.158$ and $T_{33} = 14524.574 \text{ cm}^{-1}$, and those of the $B^2 \Sigma^+ \rightarrow X^2 \Sigma^+$ system are T_{00} = 15753.585, T_{11} = 15737.733, and T_{22} = 15707.896 cm⁻¹. Since the $A^2\Pi$ state of CaH is intermediate between Hund's cases (a) and (b), six strong branches P₁₁, Q₁₁, R₁₁, P₂₂, Q₂₂ and R₂₂, and six weaker (satellite) branches P₁₂, Q₁₂, R₁₂, P₂₁, Q₂₁ and R₂₁ were observed in all $A^2\Pi \to X^2\Sigma^+$ bands. The $B^2\Sigma^+ \to X^2\Sigma^+$ bands contained four branches: P₁₁, R₁₁, P₂₂ and R₂₂; a small portion of the $B^2\Sigma^+ \rightarrow X^2\Sigma^+$ spectrum showing some *R*-branch lines is displayed in Fig. 4. Overall, our data consisted of ~3000 line positions of the $A \rightarrow X$ and $B \rightarrow X$ bands. An experimental uncertainty of 0.003 cm^{-1} was assigned to unblended lines of the 0–0. 1–1 and 2-2 bands of both electronic transitions. Lines from the 3-3, 0-1, 1–2, 2–3 and 3–4 bands of the A \rightarrow X system were relatively weak, and were given an uncertainty of 0.005 cm^{-1} . We also added ~150 line positions of the 1–0 and 2–1 bands of the $B \rightarrow X$ system from Ref. [16]. In addition, all the previous ground state data from pure rotational and vibration-rotation spectra, i.e., about 500 data used in Ref. [27], were included in our data set. A complete list of the line positions used in this study is presented in Supplementary material [50].

Table 1 The highest N values observed in vibrational levels of the $A^2\Pi$ and $B^2\Sigma^*$ states of CaH.

	$A^2\Pi$ state		$B^2\Sigma^+$ state
v	Highest N	v	Highest N
0	53	0	41
1	45	1	33
2	38	2	24
3	26		

^a N = R + L = J - S.

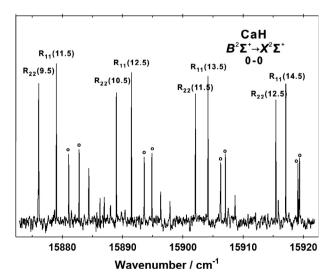


Fig. 4. A portion of the $B^2\Sigma^+ \rightarrow X^2\Sigma^+$ emission spectrum of CaH showing *R*-branch lines of the 0–0 band; the lines are marked as $R_{11}(J'')$ and $R_{22}(J'')$ in which J'' is the lower state total angular momentum quantum number; $J = N + \frac{1}{2}$ for the *f* parity. The weaker lines marked with circles are from the 1–1 band.

An effective N^2 Hamiltonian [51] was used for the ${}^2\Pi$ and ${}^2\Sigma^+$ states in our least-squares fitting program. We have recently carried out a deperturbation analysis [52] of the $A^2\Pi$ and $B'^2\Sigma^+$ states of MgH and published the N^2 Hamiltonian matrix elements for ${}^2\Pi$ state, as well as analytical energy expressions for ${}^{2}\Sigma^{+}$ states [52]. In the case of CaH, the electronic term value (T_e) of the $B^2\Sigma^+$ state is about 1350 cm⁻¹ higher than that of the A²Π state, and this difference is almost equal to vibrational level spacings of both states. As a result, the v = 0 level of the $B^2 \Sigma^+$ state is strongly perturbed by the v = 1 level of the A² Π state. More generally, vibrational levels of the $B^2\Sigma^+$ state (v_B) are all perturbed strongly by those of the $A^2\Pi$ state ($v_A = v_B + 1$). In the absence of these perturbations, the effective N^2 Hamiltonian should reproduce all the observed level energies. In order to take the perturbations into account, we constructed a Hamiltonian matrix for CaH that is almost identical to that used for MgH: the only difference is that we have added an additional parameter for CaH that allows for some centrifugal distortion in the off-diagonal constants that couple the ${}^{2}\Pi$ and ${}^{2}\Sigma^{+}$ state vibrational levels. More precisely, the $bB_{\nu_{\Pi},\nu_{\Sigma}}$ constants used in Ref. [52] have now been replaced by $bB_{\nu_{\Pi},\nu_{\Sigma}}$ + $d_{v_{\Pi},v_{\Sigma}}(J+1/2)[(J+1/2)\mp 1]$. Thus, the following off-diagonal matrix elements in which the upper (lower) sign refers to e(f) parity were used in our Hamiltonian for CaH.

$$\langle {}^{2}\Pi_{1/2} | \hat{\mathbf{H}}_{Rot} + \hat{\mathbf{H}}_{SO} | {}^{2}\Sigma_{1/2}^{+} \rangle = \frac{a_{\nu_{\Pi},\nu_{\Sigma}}}{2} + [1 \mp (J + 1/2)] \\ \times [bB_{\nu_{\Pi},\nu_{\Sigma}} + d_{\nu_{\Pi},\nu_{\Sigma}}(J + 1/2)] \\ \times [(J + 1/2) \mp 1]]$$
(1)

$$\begin{split} & \sum_{j=1}^{2} \Pi_{3/2} |\hat{\mathbf{H}}_{\mathbf{R}ot} + \hat{\mathbf{H}}_{SO}|^{2} \Sigma_{1/2}^{+} \rangle = -\sqrt{(J-1/2)(J+3/2)} \\ & \times \left[b B_{\nu_{\Pi},\nu_{\Sigma}} + d_{\nu_{\Pi},\nu_{\Sigma}} (J+1/2) \right. \\ & \times \left[(J+1/2) \mp 1 \right]] \end{split}$$

The parameters $a_{\nu_{\Pi},\nu_{\Sigma}}$ and $bB_{\nu_{\Pi},\nu_{\Sigma}}$ have been defined previously [52] for the MgH molecule. Three pairs of interacting vibrational levels (ν_{Π} , ν_{Σ}) were considered for CaH; the v = 1, 2 and 3 levels of the A² Π state are perturbed by the v = 0, 1 and 2 levels of the B² Σ^+ state, respectively.

A single Hamiltonian matrix containing all the observed vibrational levels of the A² Π and B² Σ ⁺ states was constructed, and the off-diagonal constants $a_{\nu_{\Pi},\nu_{\Sigma}}$, $bB_{\nu_{\Pi},\nu_{\Sigma}}$ and $d_{\nu_{\Pi},\nu_{\Sigma}}$ were determined for the perturbed vibrational levels (ν_{Π} , ν_{Σ}) from least-squares fitting of all the data. Instead of the usual "band constants", we used the following Dunham-type expressions for the A_{v} , γ_{v} , p_{v} and q_{v} constants:

$$A_{v} = A_{e} + \sum_{k=1}^{k} A_{k} (v + 1/2)^{k},$$
(3)

$$\gamma_{\mathbf{v}} = \gamma_{\mathbf{e}} + \sum_{k=1}^{k} \gamma_k (\boldsymbol{\nu} + 1/2)^k, \tag{4}$$

$$p_{v} = p_{e} + \sum_{k=1}^{k} p_{k} (\nu + 1/2)^{k},$$
(5)

$$q_{v} = q_{e} + \sum_{k=1}^{k} q_{k} (v + 1/2)^{k}, \tag{6}$$

Similar Dunham-type expressions were used for the higher-order parameters $\gamma_{D,v}$, $p_{D,v}$, $q_{D,v}$, etc. The vibronic term value (T_v), inertial rotational constant (B_v), and the centrifugal distortion constants (D_v , H_v , L_v and M_v) were represented by the well-known Dunham coefficients ($Y_{l,m}$). All the data were included in this Dunham-type fit, and the resulting parameters for the $X^2\Sigma^+$, $A^2\Pi$ and $B^2\Sigma^+$ states are presented in Table 2. The output of our

Table	2
-------	---

Dunham-type constants for the $X^2\Sigma^+$, $A^2\Pi$ and $B^2\Sigma^+$ states (in cm⁻¹), and the off-diagonal parameters coupling vibrational levels of the $A^2\Pi$ and $B^2\Sigma^+$ states.^a

Constant	$X^2\Sigma^+$ state	$B^2\Sigma^+$ state	$A^2\Pi$ state	Constant	$A^2\Pi$ state
Te	0.0	15756.2653(17)	14406.8772(13)	Ae	79.9241(23)
Y _{1,0}	1298.3992(10)	1296.5174(29)	1336.3226(32)	A_1	-0.0250(55)
Y _{2,0}	-19.18044(79)	-26.12074(101)	-20.2440(19)	A_2	-0.0593(33)
$10^{2} Y_{3,0}$	4.193(23)		-3.787(33)	$\overline{A_3}$	0.01617(56)
$10^3 Y_{4,0}$	-9.409(23)			pe	-0.76895(90)
Y _{0,1}	4.2770404(25)	4.474038(103)	4.364825(60)	p_1	0.08368(238)
$10^{1} Y_{1,1}$	-0.966235(65)	-1.0480(16)	-1.05982(162)	$10^2 p_2$	-4.606(136)
$10^3 Y_{2,1}$	-0.15325(421)	-4.326(58)	1.580(93)	$10^3 p_3$	9.90(23)
$10^4 Y_{3,1}^{2,1}$	0.013(11)		-4.538(151)	$10^4 p_{D,e}$	1.6335(196)
$10^5 Y_{4,1}$	-0.7587(10)			$10^4 p_{D,1}$	-1.0855(512)
$10^4 Y_{0,2}$	-1.852371(88)	-2.3171(26)	-1.84783(61)	$10^5 p_{D,2}$	5.84(31)
$10^4 Y_{1,2}$	0.00226(11)	0.2791(61)	0.0437(16)	$10^5 p_{D,3}$	-1.092(56)
$10^5 Y_{2,2}$	0.00164(39)	-1.630(26)	-0.2825(101)	$10^8 p_{H,e}$	-2.726(130)
$10^{6} Y_{3,2}$	-0.02495(46)		0.659(18)	$10^{8} p_{H,1}$	-1.31(35)
$10^{8} Y_{0.3}$	0.67617(130)	2.235(65)	0.4998(24)	$10^8 p_{H,2}$	2.16(24)
$10^{8} Y_{1.3}$	0.009275(855)	-3.365(162)	0.037(38)	$10^{8} p_{H,3}$	-0.773(52)
$10^{8} Y_{2,3}$	-0.003589(129)	1.291(72)	0.00539(136)	$10^{12} p_{L,e}$	5.53(17)
$10^{12} Y_{0,4}$	-0.3867(70)	-24.094(637)	-0.0882(91)	$10^{12} p_{L,1}$	-4.37(27)
$10^{12} Y_{1,4}$	-0.0370(23)	60.4(16)	-0.0574(36)	$10^{1} q_{e}$	-0.7006(12)
$10^{12} Y_{2,4}$		-27.408(73)		$10^{1} q_{1}$	-0.07907(337
$10^{16} Y_{0,5}$	0.116(12)	16.71(84)	-0.226(15)	$10^{3} q_{2}$	3.121(196)
$10^{16} Y_{1,5}$		-36.1(16)		$10^{4} q_{3}$	-7.307(320)
70 Г.,5 Уе	0.0442686(52)	-0.71969(79)	0.44301(49)	$10^{5} q_{D,e}$	1.1294(120)
Ye Y1	-0.001400(11)	-0.0422(11)	-0.0440(12)	$10^{5} q_{D,1}$	0.8501(337)
$10^{2} \gamma_{2}$	-0.00132(29)	3.518(41)	2.739(69)	$10^{6} q_{D,2}$	-5.374(214)
$10^{3} \gamma_{3}$. ,	5.518(41)	-5.81(11)	$10^{6} q_{D,2}$ $10^{6} q_{D,3}$	1.3004(392)
$10^4 \gamma_{D,e}$	 -0.05068(30)	0.809(18)	-0.9311(92)	$10^{9} q_{H,e}$	-2.810(31)
$10^{4} \gamma_{D,1}$	()	0.602(23)	0.736(22)	$10^{9} q_{H,1}$	-2.810(31) 0.5244(714)
$10^{5} \gamma_{D,2}$		-3.298(78)	-4.67(11)	$10^{9} q_{H,2}$	0.1394(264)
$10^{5} \gamma_{D,2}$ $10^{5} \gamma_{D,3}$			0.963(18)	$10^{13} q_{H,2}$ $10^{13} q_{L,e}$	2.321(17)
$10^{\circ} \gamma_{D,3}$ $10^{\circ} \gamma_{H,e}$	0.0242(22)	-1.80(12)	2.063(48)	$10 q_{L,e}$	2.521(17)
$10^{\circ} \gamma_{H,e}$, ,	-2.166(72)	-1.203(91)		
$10^8 \gamma_{H,1}$					
$10^8 \gamma_{H,2}$		1 29(2.4)	0.656(26)		
$10^{12} \gamma_{L,e}$ $10^{12} \gamma_{L,1}$		1.28(34)	-2.42(10)		
<u>10 γ_{L,1}</u> Off-diagonal cons	stants coupling the $A^2\Pi$ and $B^2\Sigma$	states	1.69(17)		
Constant	$v_{\rm A} = 1, v_{\rm B} = 0$		$v_{\rm A} = 2, v_{\rm B} = 1$		$v_{\rm A} = 3, v_{\rm B} = 2$
$a_{\nu_{\Pi},\nu_{\Sigma}}$		-1.694(31)		-0.891(17)	
$h_{R}^{u}v_{\Pi}, v_{\Sigma}$	-0.61889(68)		-0.78722(31)		1.270(15) -0.85762(21
$bB_{\nu_{\Pi},\nu_{\Sigma}}$ 10 ³ d	0.7326(70)		1.0926(52)		1.6666(55)
$10^3 d_{\nu_{\Pi},\nu_{\Sigma}}$	0.7326(70) 1.0926(52)				1.0000(55)

^a The numbers in parentheses are 1σ uncertainties in the last quoted digits.

least-squares fitting program, including line positions and the observed-minus-calculated values, is included in Supplementary material [50].

Although relative signs of the $a_{\nu_{\Pi},\nu_{\Sigma}}$, $bB_{\nu_{\Pi},\nu_{\Sigma}}$ and $d_{\nu_{\Pi},\nu_{\Sigma}}$ constants have been determined from the deperturbation analysis, their absolute signs (+/-) cannot be determined from spectroscopic data alone. In a recent study on Zeeman spectroscopy of CaH, the $bB_{1,0}$ constant was reported to be -0.69239(15) cm⁻¹ from analysis of some low-J lines [41]. The constants $a_{1,0}$ and $d_{1,0}$ were not included in that fit, and a negative sign was selected for $bB_{1,0}$; based on theoretical arguments [41]. We have thus decided to report negative signs for all $bB_{\nu_{\Pi},\nu_{\Sigma}}$ constants. For example, the value of $bB_{1,0}$ in our fit (Table 2) is reported as -0.61889(68) cm⁻¹, in reasonable agreement with that of Ref. [41], which was obtained from analysis of low-J lines.

The Dunham-type fit has an overall dimensionless standard error (DSE) of 0.88, which means that the 120 constants listed in Table 2 can reproduce the data within their experimental uncertainties. The $X^2\Sigma^+$, $A^2\Pi$ and $B^2\Sigma^+$ states required 24, 61 and 26 parameters, respectively, and there are 9 off-diagonal constants that couple the vibrational levels of the $A^2\Pi$ and $B^2\Sigma^+$ states. The equilibrium constants T_e , ω_e and $\omega_e x_e$ for CaH were determined to be 14406.877(1), 1336.323(3) and 20.244(2) cm⁻¹ for the $A^2\Pi$ state, and 15756.265(2), 1296.517(3) and 26.121(1) cm⁻¹ for the

B²Σ⁺ state, respectively. The equilibrium internuclear distances (*r*_e) were determined directly from the Y_{0,1} Dunham coefficients to be 2.002361(1), 1.98212(1) and 1.95778(2)Å for the X²Σ⁺, A²Π and B²Σ⁺ states, respectively.

We performed another fit in which the $X^2\Sigma^+$, $A^2\Pi$ and $B^2\Sigma^+$ states were all fitted by empirical band constants, and the off-diagonal constants $a_{\nu_{\Pi},\nu_{\Sigma}}$, $bB_{\nu_{\Pi},\nu_{\Sigma}}$ and $d_{\nu_{\Pi},\nu_{\Sigma}}$ were fixed to the values listed in Table 2. This band constant fit employed a total of 142 parameters, of which 9 were held fixed, and a DSE of 0.86 was obtained. In this case, the $X^2\Sigma^+$, $A^2\Pi$ and $B^2\Sigma^+$ states required 37, 70 and 26 parameters, respectively; the band constants are listed in Table 3, and the least-squares fitting output is included in Supplementary material [50].

Near the highest observed rotational quantum numbers, additional perturbations were observed in the vibrational levels of both $A^2\Pi$ and $B^2\Sigma^+$ states. For the v = 0, 1, 2 and 3 levels of the $A^2\Pi$ state, local perturbations are observed near N = 53, 45, 36 and 25, respectively, and the v = 1 and 2 levels of the $B^2\Sigma^+$ state are perturbed near N = 33 and 24, respectively. Some of these perturbations were reported previously by Berg and Klynning [14], and an explanation was given by Klynning and Martin [53] that the second minimum in the potential curve of the $B^2\Sigma^+$ state is responsible for them.

Table 3

Band constants for the $X^2\Sigma^+$, $A^2\Pi$ and $B^2\Sigma^+$ states of CaH (in cm⁻¹).^a

$X^2\Sigma^+$	v = 0	<i>v</i> = 1	v = 2	v = 3	v = 4
T _v	0.0	1260.1275(2)	2481.9986(2)	3665.4137(3)	4809.9462(4)
Bv	4.22869002(57)	4.1317286(25)	4.0342497(34)	3.9358901(50)	3.8361169(80
$10^4 D_{\rm v}$	1.851248(66)	1.849617(108)	1.84958(14)	1.85263(24)	1.85929(39)
$10^8 H_{\rm v}$	0.6803(11)	0.6855(17)	0.6749(19)	0.6548(39)	0.5796(51)
$10^{12} L_{v}$	-0.4077(63)	-0.4696(113)	-0.4493(79)	-0.447(19)	
$10^{16} \dot{M_v}$	0.121(12)	0.186(27)			
$10^2 \gamma_v$	4.35655(15)	4.2093(21)	4.0623(21)	3.9190(30)	3.7723(58)
$10^{6} \gamma_{DV}$	-5.075(30)	-4.973(69)	-4.797(37)	-4.929(67)	-5.10(18)
$10^{10} \gamma_{\rm H,v}$	2.47(22)	2.12(51)			
$B^2\Sigma^+$	v = 0	<i>v</i> = 1	<i>v</i> = 2	Off-diagonal	(fixed) ^b
ſ _v	15753.5849(6)	16997.8607(7)	18189.8944(96)	a _{1,0}	-1.694
, B _v	4.4205480(98)	4.307096(20)	4.185027(36)	$bB_{1,0}$	-0.61889
$10^4 D_v$	2.21792(42)	2.2651(13)	2.6441(35)	$10^3 d_{1.0}$	0.7326
$10^8 H_v$	0.8682(69)	0.092(34)	2.256(117)	a _{2,1}	-0.891
$10^{12} L_{\rm v}$	-0.690(48)	4.85(37)	-53.2(13)	$bB_{2,1}$	-0.78722
$10^{16} M_{y}$	-1.50(12)	-37.5(15)		$10^3 d_{2,1}$	1.0926
γν	-0.731554(77)	-0.70370(12)	-0.60584(22)	a _{3,2}	1.270
$10^4 \gamma_{D,v}$	1.0022(19)	0.9579(46)	0.301(18)	bB _{3.2}	-0.85762
10 ⁸ γ _{H,v}	-2.544(11)	-4.815(40)	-8.05(32)	$10^3 d_{3,2}$	1.6666
A ² Π	v = 0	<i>v</i> = 1	v = 2	<i>v</i> = 3	
T _v	14425.5638(3)	15721.2748(3)	16976.1566(5)	18189.9875(9)	
S _v	4.3121690(35)	4.2078903(41)	4.1026926(70)	3.993704(23)	
$10^4 D_v$	1.83212(12)	1.82438(12)	1.81388(28)	1.7521(16)	
$10^8 H_v$	0.5185(16)	0.5811(12)	0.6521(38)	0.535(42)	
$10^{12} L_{\rm y}$	-0.1109(84)	-0.2694(38)	-0.382(17)	1.00(36)	
$10^{16} M_{\rm v}$	-0.2365(152)				
A _v	79.89883(60)	79.80777(65)	79.74270(80)	79.8056(13)	
γv	0.427116(79)	0.41900(10)	0.41288(18)	0.37648(34)	
$10^4 \gamma_{D,v}$	-0.6674(21)	-0.5520(35)	-0.4744(92)	-0.023(19)	
10 ⁸ γ _{H,v}	1.622(18)	1.730(38)	2.64(15)	7.26(26)	
$10^{12} \gamma_{L,v}$	-1.565(45)	0.14(13)	4.47(78)		
	-0.737376(83)	-0.713742(98)	-0.69284(14)	-0.61559(28)	
p_v 10 ⁴ $p_{D,v}$	1.2225(28)	0.9568(41)	0.8436(94)	0.316(19)	
$10^{8} p_{\rm D,v}$ $10^{8} p_{\rm H,v}$	-2.931(26)	-2.532(50)	-4.12(18)	-14.98(31)	
$10^{12} p_{\rm L,v}$	3.323(71)	-0.69(17)	-8.18(97)	-14.56(31)	
$10^{1} p_{L,v}$ $10^{1} q_{v}$	-0.733263(37)	-0.773647(51)	-0.81768(10)	-0.90690(24)	
$10^{5} q_{\rm D,v}$	1.43688(94)	1.6350(16)	1.9395(48)	3.010(12)	
$10^{9} q_{\rm H,v}$	-2.5171(72)	-1.723(15)	-0.759(71)	2.02(16)	
$10^{-} q_{\rm H,v}$ $10^{13} q_{\rm L,v}$		2.379(45)	. ,	. ,	
$10 q_{L,v}$	2.331(17)	2.379(45)	2.71(33)		

^a The numbers in parentheses are 1σ uncertainties in the last quoted digits.

^b The off-diagonal constants were taken from Table 2 and held fixed in the fit.

4. Conclusions

High resolution Fourier transform emission spectra of CaH were recorded. The $\Delta v = 0$ and -1 sequences of the $A^2\Pi \rightarrow X^2\Sigma^+$ transition, and the $\Delta v = 0$ sequence of the $B^2\Sigma^+ \rightarrow X^2\Sigma^+$ band system were observed and rotationally analyzed. Deperturbation of the $A^2\Pi$ and $B^2\Sigma^+$ states were carried out using a Hamiltonian matrix that includes ${}^2\Pi$ and ${}^2\Sigma^+$ matrix elements, as well as off-diagonal elements that couple the vibrational levels of the two states. Empirical band constants and Dunham-type parameters were obtained by least-squares fitting of the data. The equilibrium constants T_e , ω_e and $\omega_e x_e$ were determined to be 14406.877(1), 1336.323(3) and 20.244(2) cm⁻¹ for the $A^2\Pi$ state, and 15756.265(2), 1296.517(3) and 26.121(1) cm⁻¹ for the $B^2\Sigma^+$ state, respectively. The equilibrium internuclear distances (r_e) of the $A^2\Pi$ and $B^2\Sigma^+$ states of CaH are 1.98212(1) and 1.95778(2) Å, respectively.

Acknowledgments

The spectra of CaH were recorded at the National Solar Observatory on Kitt Peak, AZ, and at the University of Waterloo. Support for this work was provided by a Research Project Grant from the Leverhulme Trust (UK).

Appendix A. Supplementary material

Supplementary data associated with this article can be found, in the online version, at http://dx.doi.org/10.1016/j.jms.2013.04.009.

References

- [1] C.M. Olmstead, Astrophys. J. 27 (1908) 66.
- [2] Y. Öhman, Astrophys. J. 80 (1934) 171.
- [3] R. Boyer, P. Sotirovski, J.W. Harvey, Astron. Astrophys. Suppl. 24 (1976) 111.
- [4] J.R. Mould, D.B. McElroy, Astrophys. J. 220 (1978) 935.
- [5] J.E. Gizis, Astronom. J. 113 (1997) 806.
- [6] B. Barbuy, R.P. Schlavon, J. Gregorio-Hetem, P.D. Singh, C. Batalha, Astron. Astrophys. Suppl. Ser. 101 (1993) 409.
- [7] S. Lépine, M.M. Shara, R.M. Rich, Astrophys. J. 585 (2003) L69.
- [8] S. Lépine, R.-D. Scholz, Astrophys. J. 681 (2008) L33.
- [9] R.S. Mulliken, Phys. Rev. 25 (1925) 509.
- [10] E. Hulthèn, Phys. Rev. 29 (1927) 97.
- [11] W.W. Watson, W. Bender, Phys. Rev. 35 (1930) 1513.
- [12] W. Watson, R. Weber, Phys. Rev. 48 (1935) 732.
- [13] W.W. Watson, Phys. Rev. 47 (1935) 27.
- [14] L.E. Berg, L. Klynning, Phys. Scr. 10 (1974) 331.
- [15] L.E. Berg, L. Klynning, Astron. Astrophys. Suppl. 13 (1974) 325.
 [16] L.E. Berg, L. Klynning, H. Martin, Opt. Commun. 17 (1976) 320.
- [17] H. Martin, J. Mol. Spectrosc. 108 (1984) 66.
- [18] B. Kaving, B. Lindgren, Phys. Scr. 10 (1974) 81.
- [19] B. Kaving, B. Lindgren, D.A. Ramsay, Phys. Scr. 10 (1974) 73.
- [20] B. Kaving, B. Lindgren, Phys. Scr. 13 (1976) 39.
- [21] G.D. Bell, M. Herman, J.W.C. Johns, E.R. Peck, Phys. Scr. 20 (1979) 609.
- [22] H. Martin, J. Chem. Phys. 88 (1988) 1797.

- [23] C.I. Frum, J.J. Oh, E.A. Cohen, H.M. Pickett, Astrophys. J. 408 (1993) L61.
- [24] C.I. Frum, H.M. Pickett, J. Mol. Spectrosc. 159 (1993) 329.
- [25] W.L. Barclay Jr., M.A. Anderson, L.M. Ziurys, Astrophys. J. 408 (1993) L65.
- [26] D. Petitprez, B. Lemoine, C. Demuynck, J.L. Destombes, B. Macke, J. Chem. Phys. 91 (1989) 4462.
- [27] A. Shayesteh, K.A. Walker, I. Gordon, D.R.T. Appadoo, P.F. Bernath, J. Mol. Struct. 695-696 (2004) 23.
- [28] G. Jeung, J.-P. Daudey, J.-P. Malrieu, Chem. Phys. Lett. 98 (1983) 433.
- [29] P. Fuentealba, O. Reyes, H. Stoll, H. Preuss, J. Chem. Phys. 87 (1987) 5338.
- [30] G. Chambaud, B. Levy, J. Phys. B: At., Mol. Opt. Phys. 22 (1989) 3155.
- [31] A. Boutalib, J.P. Daudey, M. El Mouhtadi, Chem. Phys. 167 (1992) 111.
- [32] N. Honjou, M. Takagi, M. Makita, K. Ohno, J. Phys. Soc. (Jpn.) 50 (1981) 2095.
- [33] L.G.M. Pettersson, P.E.M. Siegbahn, S. Ismail, Chem. Phys. 82 (1983) 355.
- [34] S. Norihiro, T. Kiyoshi, K. Ohno, J. Mol. Spectrosc. 121 (1987) 283.
- [35] T. Leininger, G.-H. Jeung, J. Chem. Phys. 103 (1995) 3942.
- [36] F. Holka, M. Urban, Chem. Phys. Lett. 426 (2006) 252.
- [37] I.S.K. Kerkines, A. Mavridis, J. Phys. Chem. A 111 (2007) 371.
- [38] P.F. Weck, P.C. Stancil, K. Kirby, J. Chem. Phys. 118 (2003) 9997.
- [39] T.C. Steimle, J. Gengler, J. Chen, Can. J. Chem. 82 (2004) 779.
- [40] T.C. Steimle, J. Chen, J. Gengler, J. Chem. Phys. 121 (2004) 829.

- [41] J. Chen, J. Gengler, T.C. Steimle, J.M. Brown, Phys. Rev. A 73 (2006) 012502.
- [42] M. Liu, T. Pauchard, M. Sjödin, O. Launila, P. van der Meulen, L.E. Berg, J. Mol. Spectrosc. 257 (2009) 105.
- [43] R.S. Ram, K. Tereszchuk, I.E. Gordon, K.A. Walker, P.F. Bernath, J. Mol. Spectrosc. 266 (2011) 86.
- [44] G. Li, J.J. Harrison, R.S. Ram, C.M. Western, P.F. Bernath, J. Quant. Spectrosc. Radiat. Trans. 113 (2012) 67.
- [45] E. GharibNezhad, A. Shayesteh, P.F. Bernath, J. Mol. Spectrosc. 281 (2012) 47. [46] B.A. Palmer, R. Engleman, Atlas of the Thorium Spectrum, Los Alamos National Laboratory, Los Alamos, NM, 1983.
- [47] T. Hirao, B. Pinchemel, P.F. Bernath, J. Mol. Spectrosc. 202 (2000) 213.
- [48] G. Norlén, Phys. Scr. 8 (1973) 249.
- [49] W. Whaling, W.H.C. Anderson, M.T. Carle, J.W. Brault, H.A. Zarem, J. Res. Natl. Inst. Stand. Technol. 107 (2002) 149.
- [50] See supplementary data at http://dx.doi.org/10.1016/j.jms.2013.04.009 for a complete list of data and constants.
- [51] J.M. Brown, E.A. Colbourn, J.K.G. Watson, F.D. Wayne, J. Mol. Spectrosc. 74 (1979) 294.
- [52] A. Shayesteh, P.F. Bernath, J. Chem. Phys. 135 (2011) 094308.
- [53] L. Klynning, H. Martin, J. Phys. B: At. Mol. Phys. 14 (1981) L365.